BBA - Bioenergetics 1860 (2019) 148054

Contents lists available at ScienceDirect

BBA - Bioenergetics

journal homepage: www.elsevier.com/locate/bbabio

# D1:Glu244 and D1:Tyr246 of the bicarbonate-binding environment of Photosystem II moderate high light susceptibility and electron transfer through the quinone-Fe-acceptor complex

Jack A. Forsman[a], Imre Vass[b], Julian J. Eaton-Rye[a,*]

[a] Department of Biochemistry, University of Otago, Dunedin 9054, New Zealand
[b] Institute of Plant Biology, Biological Research Center, Szeged, Hungary

ARTICLE INFO

*Keywords:*
Bicarbonate
Bioenergetics
D1 protein
$HCO_3^-$
Photosynthesis
Photosystem II
Cyanobacteria

ABSTRACT

In cyanobacteria, Glu-244 and Tyr-246 of the Photosystem II (PS II) D1 protein are hydrogen bonded to two water molecules that are part of a hydrogen-bond network between the bicarbonate ligand to a non-heme iron and the cytosol. Ala substitutions were introduced in *Synechocystis* sp. PCC 6803 to investigate the roles of these residues and the hydrogen-bond network on electron transfer between the primary plastoquinone acceptor, $Q_A$, and the secondary plastoquinone acceptor, $Q_B$, of the quinone-Fe-acceptor complex. All mutants assembled PS II; however, an increase in the PS II to PS I ratio was apparent, particularly in the E244A:Y246A double mutant. The mutants also showed impaired oxygen evolution and retarded chlorophyll *a* fluorescence decays following single turnover actinic flashes, which appeared to be primarily due to reduced $Q_B$ binding in the E244A strain and an enhanced back reaction with the S2 state of the oxygen-evolving complex in the Y246A mutant. Impaired PS II in the Y246A and E244A:Y246A mutants resulted in inactivation of the *psbA* gene encoding D1. The Y246A and E244A:Y246A mutants also showed high light sensitivity whereas the E244A mutant showed enhanced resilience towards photodamage. Unlike the control strain, all of the mutants were insensitive to the addition of formate or bicarbonate in assays following chlorophyll decay kinetics that reflect electron transfer between $Q_A$ and $Q_B$, suggesting the bicarbonate binding environment was perturbed. Our data also indicate that waters W582 and W622 (PDB: 4UB6) have essential roles in maintaining the architecture of the acceptor side of PS II.

## 1. Introduction

Photosystem II (PS II) catalyzes the splitting of water and reduction of plastoquinone in oxygenic photosynthesis [1,2]. This light-driven reaction transfers an electron from the P680 chlorophyll cluster of the PS II reaction center to a bound quinone acceptor ($Q_A$): this electron is then passed to a mobile quinone ($Q_B$) that is bound as $Q_B^-$. Subsequently, a second electron is transferred from P680 leading to the formation of plastoquinol ($Q_BH_2$) which then exchanges with an oxidized quinone from the plastoquinone pool in the thylakoid membrane [3,4]. The electrons that are transferred to $Q_B$ are replenished by the splitting of water that is catalyzed by a $Mn_4CaO_5$ cluster or oxygen-evolving complex (OEC) that cycles through 5 oxidation state ($S_0$ to $S_4$) with oxygen released on the $S_4$ to $S_0$ transition [5,6].

The oxidative chemistry of water splitting can lead to damage to the protein environment, and particularly to the D1 reaction center subunit that contributes ligands to the OEC, P680 and the $Q_B$ binding site [3,7]. Damage to PS II is exacerbated if either electron transfer from the OEC

*Abbreviations:* BG-11, blue-green 11 medium; BN-PAGE, blue-native polyacrylamide gel electrophoresis; CP43, 43 kDa chlorophyll-binding core antenna protein; CP47, 47 kDa chlorophyll-binding core antenna protein; DCMU, 3,4-dichloro-1,1-dimethyl urea; DMBQ, 2,5-dimethyl-1,4-benzoquinone; D1, the *psbA*-encoded reaction center protein subunit; D2, the *psbD*-encoded reaction center protein subunit; EPR, electron paramagnetic resonance; F, fluorescence level; $F_m$, maximum fluorescence level; $F_o$, initial fluorescence level; HEPES, 4-(2-hydroxyethyl)-1-piperazineethanesulfonic acid; MES, 2-(N-morpholino)ethanesulfonic acid; OEC, oxygen-evolving complex of Photosystem II; O, J, I and P, initial fluorescence level, J inflection, I inflection and peak of the fluorescence induction curve; PCC, Pasteur Culture Collection; PS II, Photosystem II; $Q_A$, primary plastoquinone electron acceptor of PS II; $Q_B$, secondary plastoquinone electron acceptor of PS II; QM/MM, quantum mechanics/molecular mechanics; ROS, reactive oxygen species; $S_{0...4}$, the oxidation states of the oxygen-evolving complex following single-turnover flashes applied to dark-adapted cells; SDS, sodium dodecyl sulfate; TES, 2-[tris(hydroxymethyl)methyl]amino-1-ethanesulfonic acid; TL, thermoluminescence; Tris, tris(hydroxymethyl)aminomethane

* Corresponding author.
*E-mail address:* julian.eaton-rye@otago.ac.nz (J.J. Eaton-Rye).

https://doi.org/10.1016/j.bbabio.2019.07.009
Received 17 April 2019; Received in revised form 12 July 2019; Accepted 18 July 2019
Available online 20 July 2019

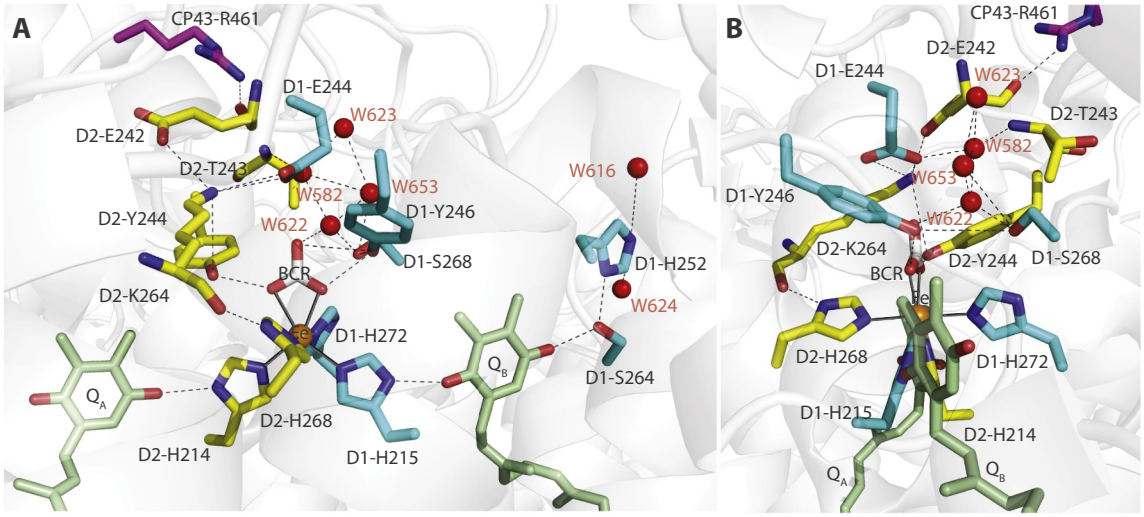


**Fig. 1.** (A) Diagram of the bicarbonate-binding environment of Photosystem II. (B) View of the bicarbonate-binding environment rotated 90° with respect to panel A with D1-H252, D1-S264, W616 and W624 omitted for clarity. The non-heme iron is shown as the orange ball. The $Q_A$ and $Q_B$ quinones are shown in green. D1 residues are shown in blue, D2 residues are shown in yellow. A CP43 residue is shown in magenta and numbered according to PDB 4UB6. Red spheres indicate waters and BCR is bicarbonate. Oxygen atoms in the amino acids, quinones and bicarbonate are shown in red. Nitrogen atoms are shown in blue. Black dashed lines represent hydrogen bonds with distances of 3.3 Å or less; however, the distances between waters W616 and W624 and D1-H252 were 4.5 and 4.3 Å, respectively. The backbone residues have been omitted for clarity unless they participate in the hydrogen-bond network. The figure was draw using PyMOL [14] and PDB 4UB6 [12].

to P680 is impaired (resulting in long-lived $P680^{+\cdot}$) or the plastoquinone pool becomes fully reduced leading to the generation of reactive oxygen species (ROS) [8,9]. Photodamaged protein resulting from these processes can be replaced but photoinhibition occurs when the rate of damage exceeds the rate of PS II repair [10].

Located between the $Q_A$ and $Q_B$ electron acceptors is a non-heme iron ligated by His ligands from D1 and the neighboring D2 reaction center subunit. In addition, a bicarbonate ion serves as a bidentate ligand to the iron [11,12] and electron transport between $Q_A$ and $Q_B$ is slowed when PS II is depleted of bicarbonate [13]. It has been hypothesized that the bicarbonate is involved in the protonation of $Q_B$ as it appears to participate in a hydrogen-bond network which connects the bicarbonate to the cytosol (or stroma in chloroplasts) (Fig. 1) [15,16]. Evidence obtained with PS II-enriched thylakoids from spinach has shown that the ligation of the bicarbonate to the non-heme iron is able to modulate the redox midpoint potential of the $Q_A/Q_A^-$ couple [17]. This has led to a proposed role for bicarbonate in photoprotection whereby accumulation of $Q_A^-$ under photoinhibitory conditions results in release of bound bicarbonate bringing about a lowering of the redox potential of $Q_A/Q_A^-$ that in turn favors a back reaction with $P680^{+\cdot}$ that avoids production of $^1O_2$ [17,18].

In this study mutagenesis of the D1 protein in the cyanobacterium *Synechocystis* sp. PCC 6803 (hereafter *Synechocystis* 6803) has been employed to investigate the roles of D1-Glu244 and D1-Tyr246 that participate in the network of hydrogen bonds linking the cytosol to bicarbonate (Fig. 1) [7,16,19].

## 2. Materials and methods

### 2.1. Strains and culture conditions

The *Synechocystis* 6803 wild type for the present study was the glucose-tolerant GT-O1 strain [20,21]. To construct mutants with substitutions in the D1 protein a deletion strain was used in which the *psbA* genes found in *Synechocystis* 6803 had been deleted and mutations were introduced into the *psbA2* copy employing kanamycin as a selectable marker [22]. Mutagenesis plasmids were constructed using the Quikchange II kit (Agilent, Santa Clara, CA, U.S.A.) and the cells were transformed and mutants verified according to Eaton-Rye [23].

Four strains were constructed: a control strain, carrying an unmodified copy of *psbA2* but possessing the selectable marker, two single mutants, E244A and Y246A, and the E244A:Y246A double mutant. The phenotype of the control strain, carrying the introduced kanamycin-resistance cassette downstream of *psbA2*, was found to be similar to wild type [22]. All strains were maintained on BG-11 media agar plates containing 5 mM glucose, 20 μM atrazine, 10 mM TES-NaOH (pH 8.2) and 0.3% sodium thiosulfate. Liquid cultures were grown mixotrophically in BG-11 media containing 5 mM glucose. In both solid and liquid media 25 μg $mL^{-1}$ kanamycin was added. Cultures were maintained at 30 °C under constant illumination at 30 μE $m^{-2} s^{-1}$.

### 2.2. Photoautotrophic growth

Cells were washed with BG-11 three times and re-suspended to an optical density at 730 nm ($OD_{730\ nm}$) of 0.05 in BG-11. The cells were grown photoautotrophically at 30 °C, with constant bubbling with air, at 30 μE $m^{-2} s^{-1}$ for low light growth curves or at 200 μE $m^{-2} s^{-1}$ for high light growth curves. The $OD_{730\ nm}$ was measured either every 12 h (low light) or every 24 h (high light).

### 2.3. Oxygen evolution assays

Cells were washed and re-suspended in BG-11 (pH 7.5) to a chlorophyll concentration of 5 μg $mL^{-1}$ and incubated on a shaker at 120 rpm under constant illumination at 30 μE $m^{-2} s^{-1}$ and 30 °C. Oxygen evolution was measured with a Clark-type electrode (Hansatech, King's Lynn, U.K.) at 30 °C using 0.2 mM 2,5-dimethyl-1,4-benzoquinone (DMBQ) and 1 mM $K_3Fe(CN)_6$. Saturating actinic light (2 mE $m^{-2} s^{-1}$) was provided by an FLS1 light source (Hansatech, King's Lynn, U.K.) passed through a Melis Griot OG 590 sharp cutoff red glass filter. High light treatments for photodamage assays were performed with 1.5 mE $m^{-2} s^{-1}$ white light from a Kodak Ektalite 1000 slide projector (Kodak, Rochester, NY, U.S.A.). Chlorophyll concentrations were determined according to MacKinney [24].

### 2.4. Low-temperature (77 K) chlorophyll a fluorescence emission spectroscopy

Cells, prepared as above, were diluted to a chlorophyll

concentration of 2.5 μg mL$^{-1}$ in BG-11 pH 7.5 and snap frozen in liquid nitrogen. Fluorescence emission spectra between 600 and 780 nm were measured on a MPF-3L fluorescence spectrophotometer (Perkins Elmer, Waltham, MA, U.S.A.) at 77 K. Spectra were collected using a scan rate of 2 nm s$^{-1}$ with excitation wavelengths of 440 nm (12 nm excitation slit width) and 580 nm (8 nm excitation slit width).

### 2.5. Variable chlorophyll a fluorescence decay measurements

Cells were washed and re-suspended in BG-11 (pH 7.5) to a chlorophyll concentration of 5 μg mL$^{-1}$ and incubated on a shaker at 120 rpm under constant illumination at 30 μE m$^{-2}$ s$^{-1}$ at 30 °C for 45 min. The cells were then dark adapted at room temperature for 2 min, prior to addition of reagents. Upon addition of the reagent the chlorophyll concentration was diluted to 2 μg mL$^{-1}$ and the sample was then further incubated for 3 min. Decay kinetics of the variable chlorophyll fluorescence yield following a single actinic flash or multiple actinic flashes were measured with a double modulation kinetic fluorometer (PSI Instruments, Brno, Czech Republic) using a blue 455 nm measuring light. The $F_o$ state in dark-adapted samples was measured by a series of three measuring flashes taken at 200 μs intervals prior to a single 30 μs saturating actinic flash or a series of actinic flashes separated by 250 ms (4 Hz), followed by a sequence of measuring pulses beginning 127 μs after the last actinic flash. The saturating light intensity was set to 100% and measuring voltage to 80%. When present, $NaHCO_2$ was at 25 mM, $NaHCO_3$ was at 15 mM, and 3-(3,4-dichlorophenyl)-1,1-dimethylurea (DCMU) was at 40 μM.

### 2.6. Variable chlorophyll a fluorescence induction

Cells were prepared as described above for the chlorophyll fluorescence decay assays and measurements were performed using the same fluorometer. Cells were illuminated under actinic light over a period of 5 s and measured using a blue 455 nm measuring light. The actinic voltage was set to 50% for all samples and the measuring light voltage was set to 80%. When present, the DCMU concentration was 40 μM.

### 2.7. Thermoluminescence measurements

Flash-induced thermoluminescence (TL) measurements were carried out essentially as described in Cser and Vass [25]. Cells equivalent to 30 μg of chlorophyll were pre-illuminated for 30 s in white light at room temperature and then cooled in darkness to −20 °C and given a single actinic flash. The sample was then cooled to −40 °C and subsequently heated to 80 °C at a rate of 20 °C min$^{-1}$. When present, DCMU was added at 60 μM.

### 2.8. Thylakoid preparation

Cells were initially washed and re-suspended in BG-11 (pH 7.5) to a chlorophyll concentration of 10 μg mL$^{-1}$ and incubated on a shaker at 120 rpm under constant illumination at 30 μE m$^{-2}$ s$^{-1}$ at 30 °C for 45 min. Cell samples (1.5 mL) were spun down at 15,000 × *g* for 1 min, the supernatant was discarded and the pellet frozen in liquid nitrogen.

To isolate thylakoid membranes, the cell pellet was thawed on ice and re-suspended in 0.25 mL of 25 mM MES-NaOH at pH 6.5, 10 mM $CaCl_2$, 10 mM $MgCl_2$, 25% (w/v) glycerol and protease inhibitor cocktail (Roche, Basel, Switzerland) (re-suspension buffer) and stored on ice. An equal volume of pre-chilled glass beads (0.1 mm, Biospec, Bartlesville, OK, U.S.A.) was added and the cells were broken using three 20 s bursts with a bead beater (Biospec, Bartlesville, OK, U.S.A.). The suspension was then spun at 900 × *g* for 1 min and supernatants were transferred and spun again at 3000 × *g* for 1 min, then transferred again and finally spun at 16000 × *g* for 15 min. The thylakoid pellets were re-suspended in 100 μL of re-suspension buffer and solubilized with an equal volume of 2% (v/v) dodecyl-β-D-maltoside; these samples were then incubated for 1 min on ice and then insoluble material was pelleted by centrifugation at 16000 × *g* for 15 min at 4 °C and the supernatant transferred to a new microfuge tube before loading.

### 2.9. Protein electrophoresis and analysis

Blue-native polyacrylamide gel electrophoresis (BN-PAGE) was performed according to Schägger [26]. Solubilized thylakoid membranes containing 1 μg of chlorophyll were separated using a 3–12% polyacrylamide gradient gel. Electrophoresis was performed using a Protean II cell (Bio-Rad Laboratories, Hercules, CA, U.S.A.) at 4 °C and 150 V for 4 h. For immunodetection assays, gels were soaked for 10 min in SDS-transfer buffer (25 mM Tris, 192 mM glycine, 20% methanol, 0.1% SDS) then transferred to polyvinylidene difluoride membrane and probed with an antibody specific to D1.

## 3. Results

### 3.1. Mutant verification

Complete segregation of the mutations introduced into the *psbA* deletion mutant of *Synechocystis* 6803 was verified by PCR. Additionally, the *psbA2* genes of the different strains were sequenced to confirm the presence of the mutations (data not shown). The locations of the D1:Glu244 and D1:Tyr246 residues and the surrounding hydrogen-bond network are shown in Fig. 1.

### 3.2. Photoautotrophic growth and assembly

The photoautotrophic doubling times for the control and E244A strains were 15 h and 25 h, respectively, and the Y246A and E244A:Y246A strains exhibited doubling times of 41 h and 47 h, respectively (Fig. 2A). BN-PAGE was performed on isolated thylakoids to assess the assembly of PS II in the mutants (Fig. 2B). A western blot, using an antibody specific to the D1 protein, showed similar levels of the PS II dimer and monomer in the mutants and the control strain (Fig. 2C).

### 3.3. Low-temperature (77 K) fluorescence emission spectroscopy

To further probe PS II assembly, low-temperature fluorescence emission spectra were measured following 440 nm excitation (Fig. 3A), which directly excites chlorophyll *a*, or 580 nm excitation (Fig. B), which excites the phycobilisome pigments. Following excitation at 440 nm, the PS II-specific emission peaks at 685 nm and 695 nm were higher in the mutants than in the control, and when normalized to the total fluorescence, the PS I-specific peak at 725 nm was lower in the mutants. The PS II emission at 685 nm from the E244A and Y246A strains increased by 24% and 23%, respectively, compared to the control, with a similar increase also observed at 695 nm. In the case of the E244A:Y246A double mutant, the 685 nm emission increased by approximately 65% relative to the control, also with a similar increase observed at 695 nm. Conversely, the emission at 725 nm dropped in the E244A, Y246A and E244A:Y246A mutants to 95%, 93% and 80% of the control peak for PS I, respectively.

With 580 nm excitation, the low-temperature fluorescence emission spectra had an increased 695 nm shoulder in the mutants, originating from PS II, in agreement with the spectra obtained with 440 nm excitation. In addition, a concomitant drop in the 725 nm (PS I) emission was observed. As seen with 440 nm excitation the most prominent change in fluorescence emission was from the double mutant which showed a 17% increase in the 695 nm shoulder relative to the 695 nm emission from the control strain, while the 730 nm peak fell to 80%.

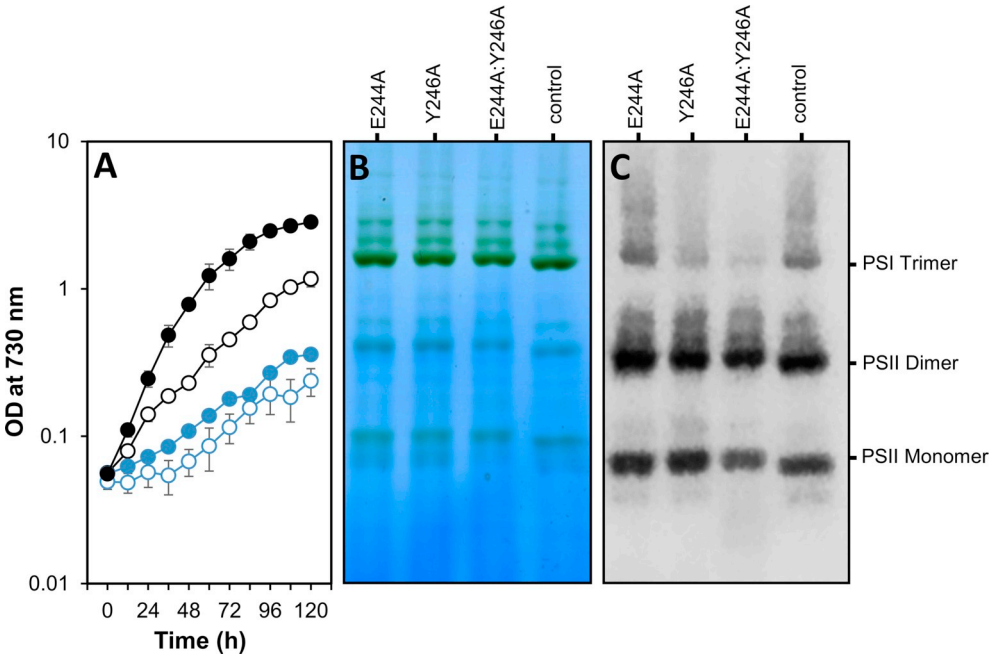


**Fig. 2.** The effects of the D1 point mutations on photoautotrophic growth and assembly. (A) Photoautotrophic growth curve determined by light scattering at 730 nm. Error bars represent the standard error from at least 3 independent experiments. Control (black filled circles), E244A (black empty circles), Y246A (blue filled circles), E244A:Y246A (blue empty circles). (B) Blue-native PAGE with 1 μg of solubilized thylakoid membranes from E244A (lane 1), Y246A (lane 2), E244A:Y246A (lane 3), control (lane 4). (C) Western blot of the blue-native PAGE gel from panel B obtained with an antibody to D1.

### 3.4. Steady-state PS II activity

Photosystem II activity was determined by measuring oxygen evolution in the presence of DMBQ (Fig. 4A). The rates of oxygen evolution in the Y246A and E244A:Y246A mutants dropped to 35% and 42% of the control rate, respectively, while the rate for the E244A strain dropped to 65%. Since the reduced oxygen evolution capacity was likely due to an impaired acceptor side in the mutants, variable chlorophyll fluorescence induction assays were performed, in the presence and absence of the PS II-specific herbicide DCMU, to assess the extent of inhibition. In the absence of DCMU (Fig. 4B), the control strain exhibited a characteristic fluorescence induction curve, made up of an initial rise to the J-level, due to $Q_A$ reduction, followed by a rise from an inflection (I) to a maximum P level as the available electron acceptors became reduced. The fluorescence then declined as a result of the activation of the Calvin-Benson cycle along with various quenching mechanisms [27]. When compared to the control strain, all of the mutants exhibited an increased O-J rise; however, while the Y246A cells reached a similar P level to control cells both the E224A mutant and the E244A:Y246A double mutant displayed an elevated P peak.

When DCMU was added (Fig. 4C) fluorescence rapidly rose to $F_m$ in all strains due to the inhibition of forward electron transfer from $Q_A^-$. The variable fluorescence yield in the presence of DCMU is typically indicative of the number of active PS II centers present. Interestingly, the fluorescence yield from the mutants exceeded that of the control strain by different amounts. The Y246A mutant showed an $F_m$ only slightly above that of the control strain; however, the fluorescence yield for E244A cells was ~25% above the control trace and the fluorescence yield from the E244A:Y246A double mutant was ~50% higher than observed with the control cells.

### 3.5. Decay of variable chlorophyll a fluorescence

To further probe the acceptor side, the decay of variable fluorescence following a single actinic flash was measured in the presence and absence of DCMU (Fig. 5). In the absence of DCMU the mutants all exhibited an increased variable fluorescence yield and retarded decay kinetics compared to the control, in agreement with the fluorescence induction results (Fig. 5A, B). The variable fluorescence decay can be divided into three kinetically distinct components: a fast (μs) phase,

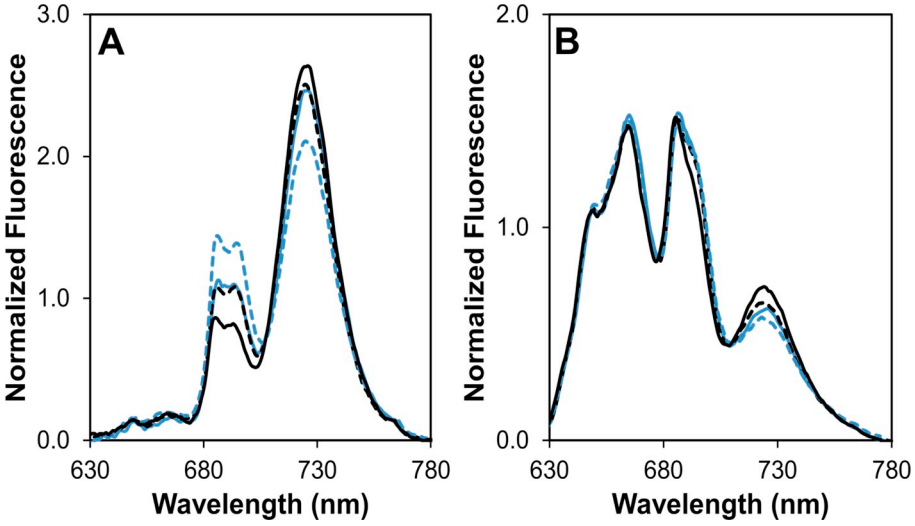


**Fig. 3.** 77 K fluorescence emission spectra. (A) 440 nm excitation and (B) 580 nm excitation for control (black solid line), E244A (black dashed line), Y246A (blue solid line), E244A:Y246A (blue dashed line). Spectra are the average of at least three independent experiments and are normalized to the total area under the spectra to reveal the ratio of the emission from PS I and PS II in each strain.

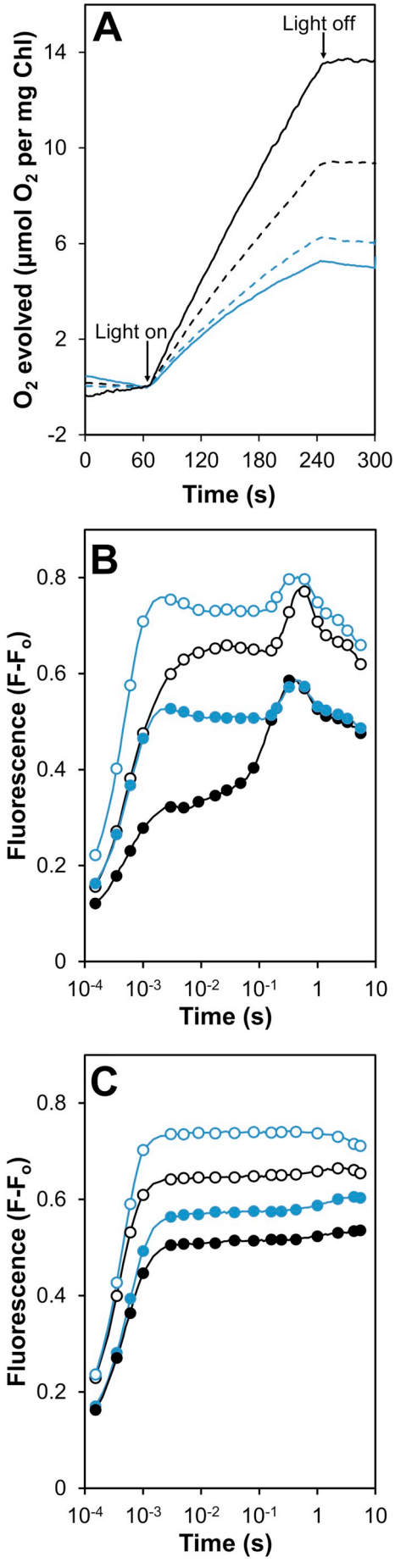


**Fig. 4.** (A) Oxygen evolution traces for control (black solid line), E244A (black dashed line), Y246A (blue solid line), E244A:Y246A (blue dashed line). The cells were treated with 200 µM DMBQ and 1 mM $K_3Fe(CN)_6$ added 90 s before the light was switched on. All cells were at a chlorophyll concentration of 5 µg $mL^{-1}$. (B) Variable chlorophyll fluorescence induction with 455 nm actinic light and measured with blue measuring flashes (455 nm). The strains were control (filled black symbols), E244A (empty black symbols), Y246A (filled blue symbols), E244A:Y246A (empty blue symbols). (C) Variable chlorophyll fluorescence induction as shown in panel B but with addition of 40 µM DCMU 2 min prior to measurement. For clarity, only selected data points are shown in panels B and C. In panel A the traces are the average of 3 independent experiments. In panels B and C the data displayed are the average of at least 4 independent experiments.

ascribed to oxidation of $Q_A^-$ by $Q_B$, an intermediate (ms) phase, ascribed to $Q_B$ binding and subsequent oxidation of $Q_A^-$, and a slow (s) phase, corresponding to the back reaction of $Q_A^-$ with the $S_2$-state of the OEC [28]. The kinetic analysis for Fig. 5 is shown in Table 1.

The E244A mutant demonstrated minor changes in the fast and slow phases of its fluorescence decay with a slight increase in the fast phase half time ($t_{1/2}$: 290 µs in control; 339 µs in E244A cells) and a small decrease in the slow phase amplitude (10% in control; 7% in the E244A strain). However, the $t_{1/2}$ of the intermediate phase for the E244A mutant exhibited an approximate 14-fold increase relative to the control ($t_{1/2}$: 5.5 ms in control; 74.3 ms in E244A cells); but there was only a small increase in the amplitude (Table 1).

The Y246A mutant demonstrated an approximate three-fold increase in the fast phase rate ($t_{1/2}$: 923 µs in Y246A cells) while the fast phase amplitude dropped to approximately half that of the control (68% in control; 29% in the Y246A strain). This coincides with an approximate six-fold decrease in the slow phase half time ($t_{1/2}$: 8.1 s in control; 1.4 s in the Y246A strain) along with a rise in the slow phase amplitude (10% in control; 59% in the Y246A mutant). The decay of the intermediate phase for the Y246 mutant ($t_{1/2}$: 16.6 ms in Y246A cells) demonstrated a proportionally similar increase to the fast phase while the amplitude of the intermediate phase also decreased (22% in the control; 12% in Y246A cells) (Table 1).

As seen in the Y246A mutant, the E244A:Y246A strain also demonstrated a slowing down of the fast phase, although to a lesser extent than in the Y246A mutant ($t_{1/2}$: 669 µs in E244A:Y246A cells) while the amplitude also dropped to approximately half of that in the control. The E244A:Y246A strain also demonstrated an acceleration in the slow phase ($t_{1/2}$: 2.3 s in E244A:Y246A cells) and an increase in the slow phase amplitude was apparent. The decay of the intermediate phase of the E244A:Y246A mutant increased to a similar extent to the fast phase, demonstrating approximately a two-fold increase ($t_{1/2}$: 13.8 ms in E244A:Y246A cells), while the amplitude of the intermediate phase remained unchanged relative to the control. It is interesting to note that the double mutant lacked the slowed intermediate phase seen in the E244A single mutant, while the amplitude shift favoring the slow phase over the fast phase in the Y246A mutant was also less pronounced in the E244A:Y246A mutant than in the Y246A strain.

In the presence of DCMU (Fig. 5C), the mutant strains exhibit increased variable fluorescence compared to the control, with the E244A, Y246A and E244A:Y246A strains showing $F_m$ levels approximately 25%, 15% and 50% higher than the control, respectively, while possessing relatively similar $F_o$ levels. The increase in variable fluorescence was consistent with the observed fluorescence induction and low-temperature fluorescence emission results (Figs. 3 and 4B, C). When normalized to $F_m$ (Fig. 5D) it is apparent that the E244A and E244A:Y246A mutants have a slower decay of variable fluorescence in the presence of DCMU (Fig. 5D and Table 1). In the presence of DCMU, $Q_A^-$ to $Q_B$ electron transfer is blocked and the decay kinetics exhibit an intermediate (ms) phase most likely arising from recombination with $P680^{+\cdot}$ and a slow (s) component, arising from recombination with $S_2$ [28].

The slow phase for the Y246A mutant was similar to the control rate when DCMU was present, with only a small change in amplitude (92%

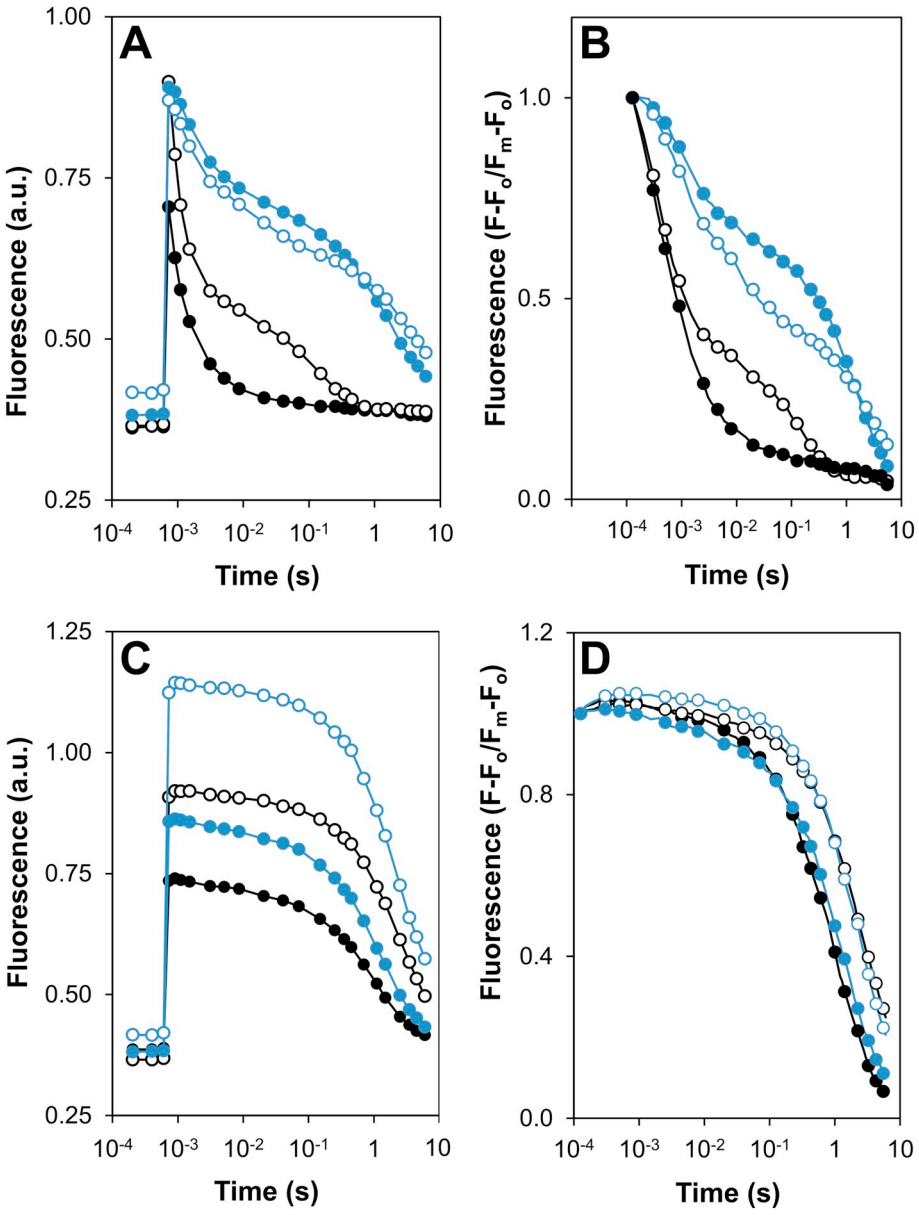


**Fig. 5.** Variable chlorophyll fluorescence relaxation following a single turnover actinic flash. For clarity only selected data points are shown. The strains are: control (filled black symbols), E244A (empty black symbols), Y246A (filled blue symbols), E244A:Y246A (empty blue symbols). Cells were dark adapted for 5 min before measurement. (A) Fluorescence decays following three determinations of $F_o$ before the actinic flash. The fluorescence was obtained with 455 nm measuring flashes. (B) Fluorescence decays from panel A normalized to $F_m$. (C) Fluorescence decays obtained as in panel A but in the presence of DCMU. (D). Fluorescence decays from panel C normalized to $F_m$. Data displayed are the average of at least 3 independent experiments.

in control; 96% in the Y246A strain). The intermediate phase was also similar ($t_{1/2}$: 6.6 ms in control; 5.8 ms in Y246A cells). In contrast, both the E244A and E244A:Y246A mutants exhibited an approximate two-fold increase in the slow phase relative to the control ($t_{1/2}$: 0.8 s in control; 2.2 s in E244A cells; and 1.9 s in the E244A:Y246A mutant), but the corresponding amplitudes remained similar (Table 1). Likewise, the intermediate phase of the E244A and E244A:Y246A mutants demonstrated an approximate two-fold increase in rate ($t_{1/2}$: 6.6 ms in control;

**Table 1**
Decay kinetics of flash-induced variable fluorescence after a single turnover flash in the presence or absence of DCMU[a].

| Strain | Treatment | Fast component | | Intermediate component | | Slow component | |
|---|---|---|---|---|---|---|---|
| | | Rate ($t_{1/2}$ = μs) | Amplitude (%) | Rate ($t_{1/2}$ = ms) | Amplitude (%) | Rate ($t_{1/2}$ = s) | Amplitude (%) |
| Control | No treatment | 290 ± 21 | 68.0 ± 1.3 | 5.5 ± 1.8 | 22.2 ± 1.6 | 8.1 ± 1.3 | 9.8 ± 0.6 |
| | +DCMU | | | 6.6 ± 0.3 | 5.6 ± 0.3 | 0.8 ± 0.1 | 92.3 ± 0.3 |
| E244A | No treatment | 339 ± 11 | 66.8 ± 0.3 | 74.3 ± 8.4 | 26.4 ± 0.1 | 7.4 ± 0.9 | 6.8 ± 0.2 |
| | +DCMU | | | 12.4 ± 4.5 | 3.1 ± 0.2 | 2.2 ± 0.1 | 96.7 ± 0.3 |
| Y246A | No treatment | 923 ± 31 | 28.9 ± 0.6 | 16.6 ± 2.5 | 12.0 ± 0.5 | 1.4 ± 0.1 | 59.1 ± 0.9 |
| | +DCMU | | | 5.8 ± 0.7 | 3.2 ± 0.7 | 0.9 ± 0.1 | 95.8 ± 0.2 |
| E244A:Y246A | No treatment | 669 ± 15 | 33.9 ± 0.6 | 13.8 ± 0.3 | 22.9 ± 0.1 | 2.3 ± 0.1 | 43.1 ± 0.7 |
| | +DCMU | | | 11.9 ± 2.8 | 2.1 ± 0.2 | 1.9 ± 0.1 | 97.8 ± 0.2 |

[a] The *Synechocystis* sp. PCC 6803 cells were either untreated or treatment with 40 μM DCMU. The fluorescence decays were analyzed according to Vass et al. [28]. Standard errors for the calculated rates and amplitudes are shown.

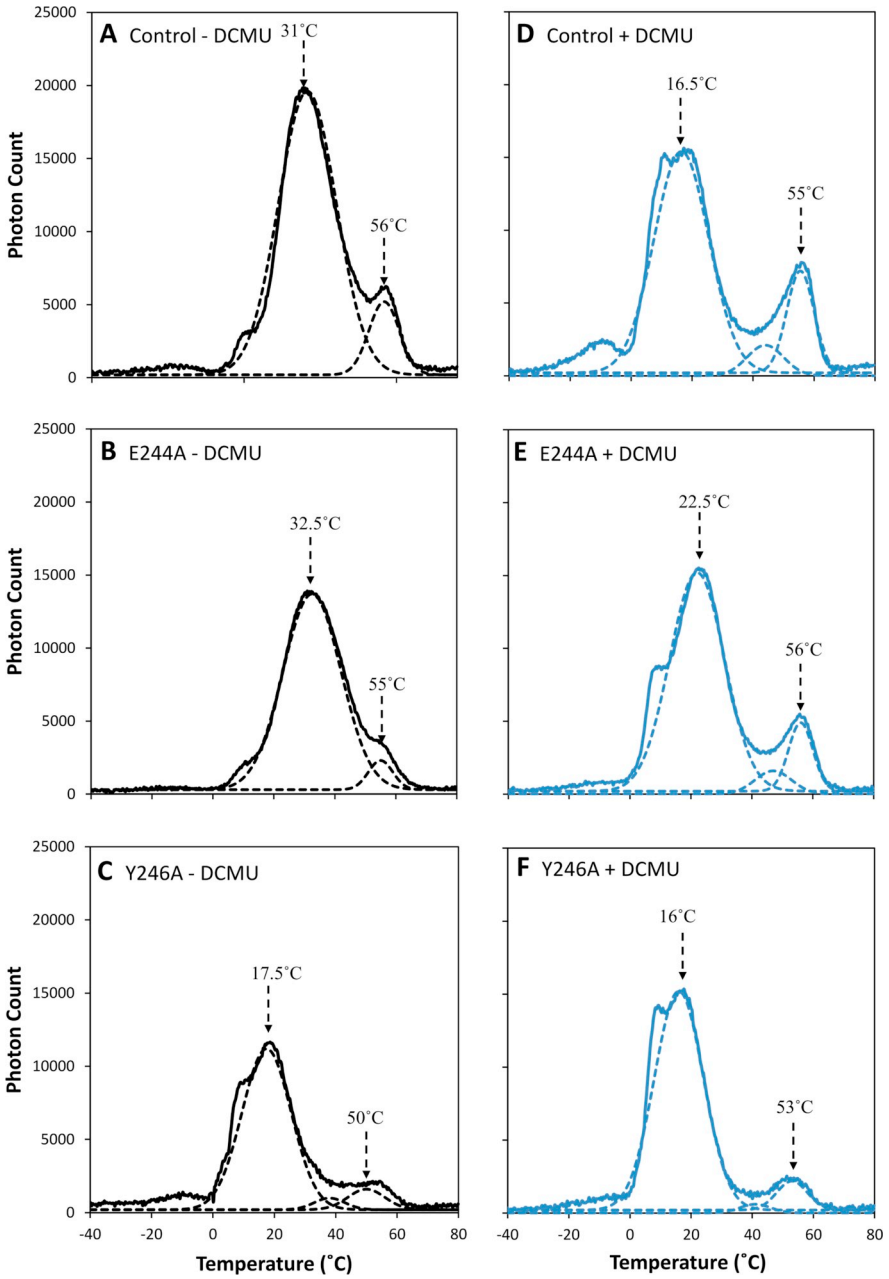


**Fig. 6.** Thermoluminescence emission from *Synechocystis* sp. PCC 6803 cells. The measured emission curves are shown in solid lines while the derived individual components which make up with total emission are shown in dashed lines. Strains were the untreated control (A), E244A (B), Y246A (C); or the control (D), E244A (E), Y246A (F) treated with 40 μM DCMU. Data displayed are the average of 3 independent experiments.

12.4 ms in E244A cells; 11.9 ms in E244A:Y246A cells), while the amplitudes only varied slightly in accordance with the variation in the amplitudes of the slow component (Table 1).

### 3.6. Thermoluminescence

To investigate the impact of the mutations in the E244A and Y246A mutants on charge recombination in PS II, TL assays were performed. Excitation of the control strain by a single flash yielded two TL peaks (Fig. 6A); a large peak at 31 °C and a smaller peak at 56 °C which correspond to the B and C bands, arising from $S_{2(3)}Q_B^-$ and Tyr-$D^{(ox)}Q_A^-$ recombination, respectively. The E244A mutant (Fig. 6B) showed a slight temperature increase in the B band and a drop in the C band to 32.5 °C and 55 °C, respectively. In the case of the Y246A mutant (Fig. 6C), the B band was replaced by a peak at 17.5 °C, which corresponds to a Q band arising from the recombination of $S_2Q_A^-$. In addition, the C band exhibited a temperature shift to 50 °C.

In the control strain, the addition of DCMU resulted in a Q band at 16.5 °C, and a C band at 55 °C (Fig. 6D). In contrast, both TL peaks in the E244A mutant were at higher temperatures than in the control, displaying a Q band at 22.5 °C and a C band at 56 °C when DCMU was present (Fig. 6E). Conversely, the Q band of the Y246A mutant in the presence of DCMU remained similar to the control, appearing at 16 °C, while the C band peak temperature decreased to 53 °C (Fig. 6F). Hence, the TL spectra for the Y246A mutant in the presence and absence of DCMU were similar.

### 3.7. Influence of formate and bicarbonate on chlorophyll fluorescence decay kinetics

Since D1:Glu244 and D1:Tyr246 participate in the hydrogen-bond network involving the bicarbonate bound to the non-heme iron the

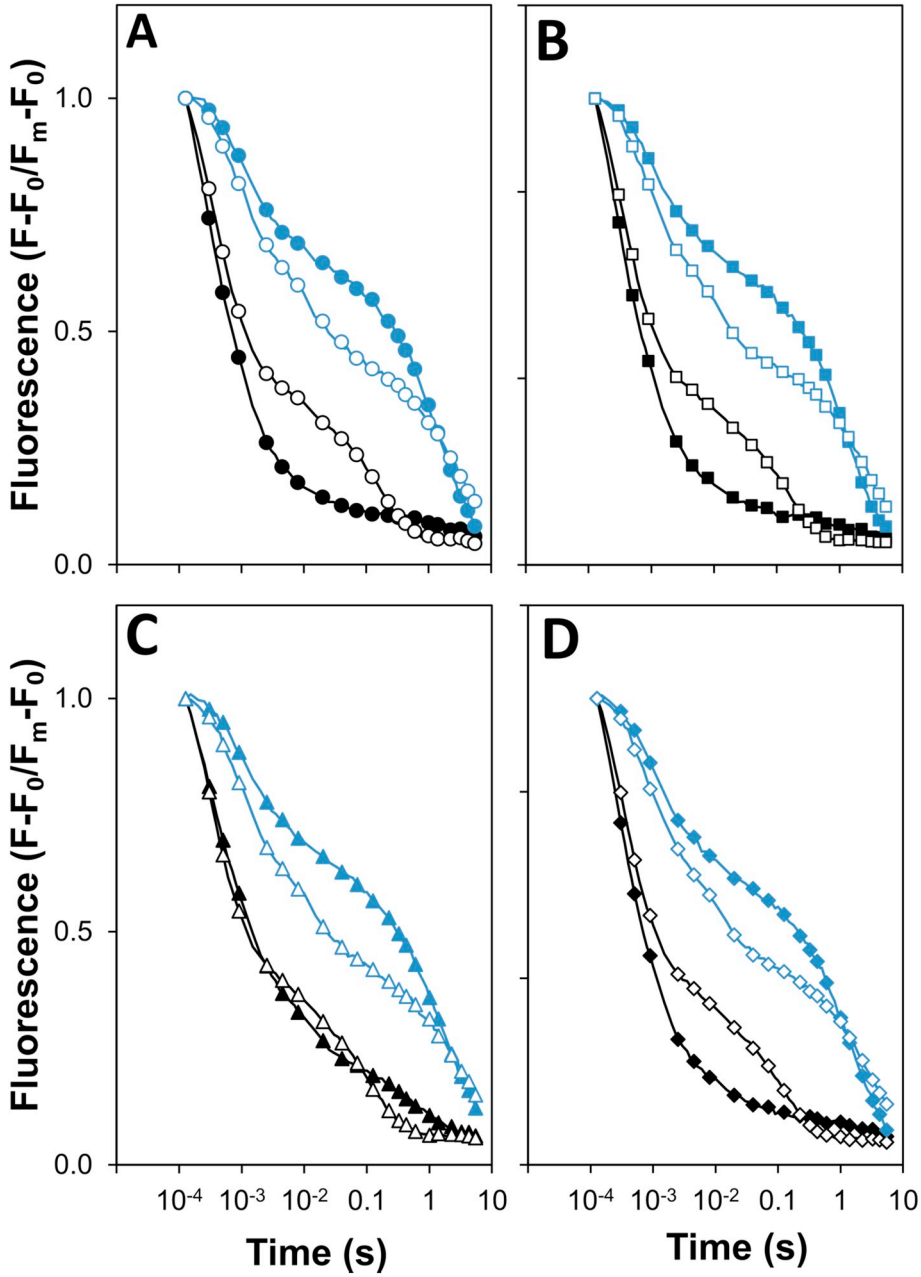


**Fig. 7.** The effect of bicarbonate and formate addition on the variable chlorophyll fluorescence relaxation following a single turnover actinic flash. The strains are: wild type (filled black symbols), E244A (empty black symbols), Y246A (filled blue symbols), E244A:Y246A (empty blue symbols). Dark-adapted cells were treated 3 min prior to measurement with: (A) no treatment; (B) 15 mM bicarbonate; (C) 25 mM formate; (D) 15 mM bicarbonate and 25 mM formate. Data displayed are the average of at least 3 independent experiments.

addition of bicarbonate was tested to see if it could recover the impaired chlorophyll fluorescence decay kinetics observed in the E244A, Y246A and E244A:Y246A mutants; however, bicarbonate did not reverse the observed inhibition (Fig. 7A, B). In the wild type, the addition of formate resulted in a reduction in the rate of fluorescence decay. This formate-induced phenotype has been ascribed to competitive binding of the formate to the non-heme iron, potentially displacing the bicarbonate and resulting in slowed $Q_A^-$ to $Q_B$ electron transfer [13,29,30]. The formate-induced phenotype was observed in wild type and reversed by bicarbonate addition (Fig. 7C, D) and similar results were obtained with control cells (not shown). However, all of the mutants were insensitive to both formate and bicarbonate, demonstrating no change in their fluorescence decay kinetics (Fig. 7B–D). In addition, the E244A cells remained insensitive to the addition of formate and bicarbonate after three actinic flashes were given to turnover the two-electron gate (Fig. 8A, B): and similarly the impact of formate and bicarbonate was slight in the Y246A and E244A:Y246A mutants following three actinic flashes (Fig. 8C, D).

### 3.8. High light sensitivity

The acceptor side of PS II is frequently damaged in high light conditions, and previous studies have observed increased high light sensitivity in acceptor side mutants [9,31]. Consequently, the tolerance of the mutant strains to high light was determined with a high light (200 $\mu E\ m^{-2}\ s^{-1}$) photoautotrophic growth curve (Fig. 9A). The control and the E244A strain grew with a doubling time of 10 h and 11 h, respectively, while the Y246A and E244A:Y246A mutants were unable to grow photoautotrophically in the high light conditions.

To investigate the high light sensitivity of the mutants on a shorter

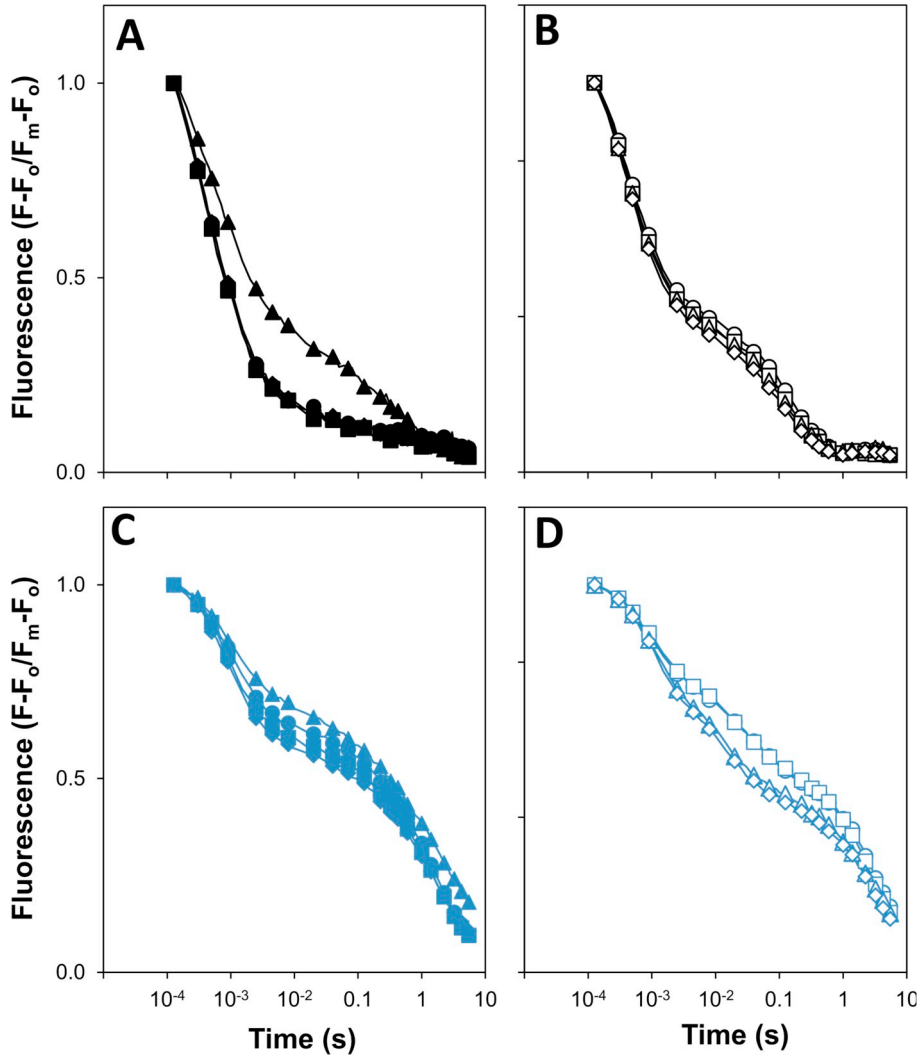


**Fig. 8.** The effect of bicarbonate and formate addition on the variable chlorophyll fluorescence relaxation following three saturating actinic flashes given at 4 Hz. The strains are: control (A, full black symbols), E244A (B, empty black symbols), Y246A (C, full blue symbols), E244A:Y246A (D, empty blue symbols). Dark-adapted cells were treated 3 min prior to measurement with: no treatment (circles); 15 mM bicarbonate (squares); 25 mM formate (triangles); 15 mM bicarbonate and 25 mM formate (diamonds). Data displayed are the average of at least 3 independent experiments.

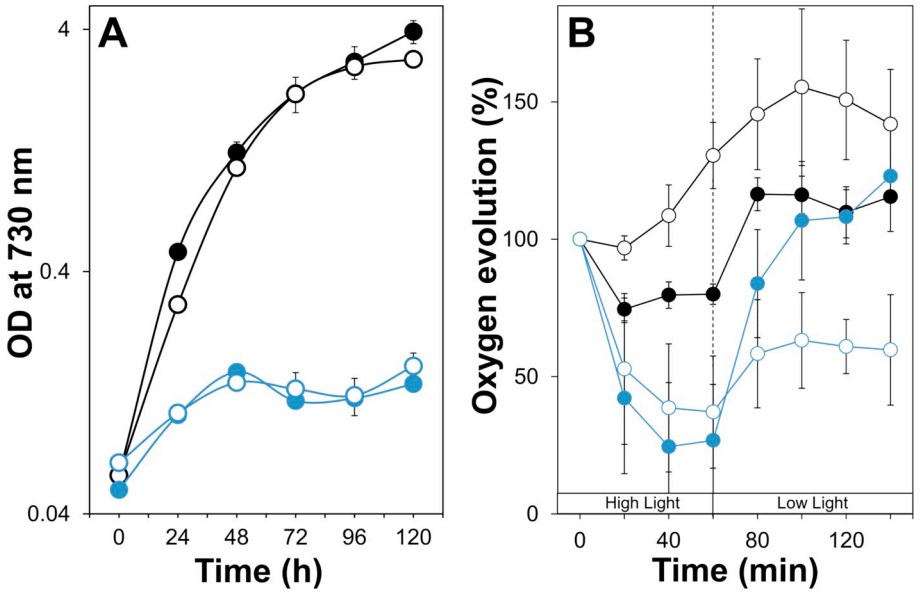


**Fig. 9.** (A) Photoautotrophic growth curve in high light (200 μE $m^{-2}s^{-1}$) determined by light scattering at 730 nm. Control (filled black symbols), E244A (empty black symbols), Y246A (filled blue symbols), E244A:Y246A (empty blue symbols). (B) Time course of oxygen evolution rates for control (filled black symbols), E244A (empty black symbols), Y246A (filled blue symbols), E244A:Y246A (empty blue symbols) during a 60 min high light (1500 μE $m^{-2}s^{-1}$) period and 80 min recovery period (30 μE $m^{-2}s^{-1}$). Oxygen evolution rates were normalized to the initial rate at time zero and determined in the presence of 200 μM DMBQ and 1 mM $K_3Fe(CN)_6$. Error bars in panels A and B represent the standard error from at least 3 independent experiments.

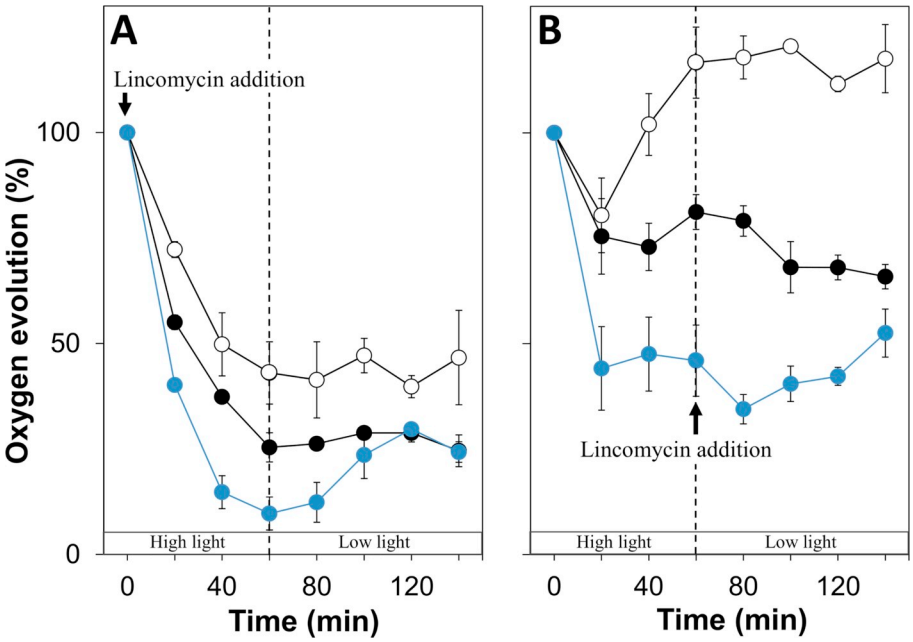


**Fig. 10.** The effect of lincomycin addition during high light and recovery from photodamage in control (filled black symbols), E244A (empty black symbols) and Y246A (filled blue symbols). All strains were treated as in Fig. 9. (A) Lincomycin added at the onset of the high light treatment. (B) Lincomycin added at the onset of the low light recovery period. Error bars in panels A and B represent the standard error from at least 3 independent experiments.

time scale, the PS II activity of the mutants was determined by measuring oxygen evolution during a high light treatment followed by a low light recovery period (Fig. 9B). The rate of oxygen evolution in the control strain remained constant during the high light treatment; however, during the low light recovery the rate of oxygen evolution in the control strain rose to approximately 130% of the initial rate. The E244A mutant was also able to tolerate the high light, as the rate of oxygen evolution consistently rose during the high light treatment, eventually peaking at 40 min into the low light recovery at approximately 150% of the initial rate of oxygen evolution. In contrast, the Y246A mutant exhibited sensitivity to high light, rapidly losing oxygen-evolving capacity in high light that dropped to approximately 20% of the initial rate during the high light treatment, before recovering to approximately the initial rate over the course of the recovery period. In contrast, the E244A:Y246A mutant was less sensitive to the high light than the Y246A mutant, with oxygen-evolving activity dropping to approximately 45% of the initial rate during the high light treatment. However, the recovery of oxygen-evolving activity in the E244A:Y246A mutant was less than in the Y246A mutant, rising to only 60% of the initial rate during the low light recovery period.

The susceptibility of control cells and the E244A and Y246A mutants to high light was compared in the presence of lincomycin to block protein synthesis. In Fig. 10A, E244A cells were found to be more resistant to high-light-induced damage than the control while Y246 cells were more sensitive. In the case of Y246A cells, a slight protein-synthesis-independent recovery was also apparent following the transition from high to low light. In addition, the observed recovery of the Y246A mutant in Fig. 9B was blocked by the addition of lincomycin following the high light treatment (Fig. 10B).

### 3.9. Spontaneous loss of PS II activity

Over the course of this study, both the Y246A and E244A:Y246A mutants lost their ability to grow photoautotrophically due to the introduction of suppressor mutations. Phenotypic analysis demonstrated a complete loss of variable fluorescence in these strains (Fig. 11A). Low-temperature fluorescence spectroscopy following 440 nm excitation (Fig. 11B), showed a loss of the 695 nm peak in both mutants with a concomitant increase in the 685 nm peak. Using 580 nm excitation, both strains exhibited increased emission at 685 nm compared to their original phenotypes (Fig. 11C). Together these results indicated an absence of assembled PS II centers in both strains. The Y246A strain displaying this new phenotype was renamed Y246A$^{sup}$ and the E244A:Y246A strain displaying this new phenotype was renamed E244A:Y246A$^{sup}$.

The genomes of the Y246A$^{sup}$ and E244A:Y246A$^{sup}$ strains were sequenced. Analysis revealed a single nucleotide polymorphism in the Y246A$^{sup}$ strain resulting in a mutation within the codon for Leu91 in the *psbA2* gene coding for a stop codon. In the case of the E244A:Y246A$^{sup}$ mutant, the *psbA2* gene contained an 8 bp insertion 703 bp into the 1100 bp *psbA2* open reading frame, resulting in a frameshift mutation. These results are summarized in Fig. S1.

## 4. Discussion

### 4.1. D1-Glu244 and D1-Tyr246 are involved in a hydrogen-bond network between bicarbonate and the cytosol

Protein structures of PS II from *Thermosynechococcus elongatus* and *T. vulcanus* have established that bicarbonate is a bidentate ligand to the non-heme iron (Fig. 1) [7,12,32]. Bicarbonate participates in a hydrogen-bond network that connects bicarbonate to the cytosol and it has been hypothesized that this network could supply protons for proton-coupled electron transfer between $Q_A$ and $Q_B$ [7]. One scenario is that $Q_B^-$ could be protonated via a hydrogen-bond network incorporating D1-His252 and D1-Ser264 while the second proton, forming the fully reduced quinol, could be supplied from bicarbonate via D1-His215 [16,33]. The suggestion that the first proton is delivered via D1-His252 and the second via bicarbonate through D1-His215 has been supported by QM/MM calculations [15].

Two key waters in the hydrogen-bond network from the cytosol to bicarbonate are waters W582 and W622 in PDB 4UB6. Water W582 is distal to bicarbonate and hydrogen bonds with water W623 (in proximity to the cytosol (Fig. 1)), as well as to D2-Thr243, D1-Glu244 and water W622. Water W622 also forms hydrogen bonds with bicarbonate, D1-Ser268 and D1-Tyr246. In this study we have introduced Ala substitutions at D1-Glu244 and D1-Tyr246 to evaluate the in vivo impact of disrupting the hydrogen-bond network on the reactions forming $Q_B^-(H^+)$, $Q_BH_2$ and the exchange of $Q_BH_2$ with the plastoquinol pool in the thylakoid membrane.

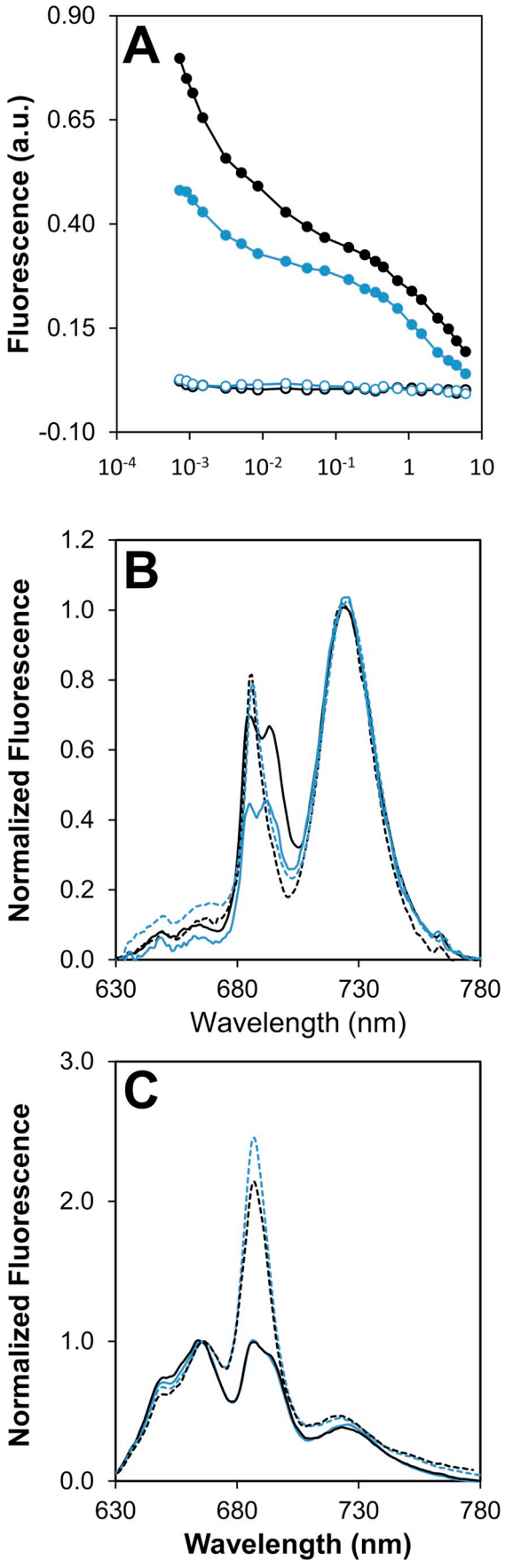


**Fig. 11.** Comparison of E244A:Y246A (full black circles or black line), Y246A (full blue circles or blue line), E244A:Y246A$^{sup}$ (empty black circles or dashed black line), Y246A$^{sup}$ (empty blue circles or dashed blue line). (A) Variable chlorophyll fluorescence relaxation following a single turnover actinic flash. (B) 77 K fluorescence emission spectra after excitation at 440 nm and normalized to PS I emission at 725 nm. (C) 77 K fluorescence emission spectra after excitation at 580 nm and normalized to phycocyanin emission at 660 nm. Data displayed are the average of at least 3 independent experiments.

### *4.2. The E244A mutant assembles PS II with altered $Q_B$ binding and is tolerant of high light*

Photoautotrophic growth of the E244A mutant and PS II assembly in this strain were similar to the control (Fig. 2). In addition, the E244A cells were less susceptible to high-light-induced photoinhibition or photodamage (Figs. 9 and 10) and exhibited relative oxygen-evolving activity above control cells in response to the high light treatment when supported by DMBQ (Figs. 9B and 10B). Dark-adapted cells of the E244A mutant, however, exhibited an approximate 14-fold increase in the rate of the intermediate component for the decay of chlorophyll fluorescence following a single actinic flash, indicative of an altered $Q_B$-binding environment (Fig. 5A, B). The fraction of centers undergoing an apparent back reaction with S2, however, was similar to that seen in control cells (Table 1) although an increase of 6 °C for the TL Q-band was observed (Fig. 6D, E). The stabilization of $Q_A^-$, implied by these TL data, was consistent with the slowed kinetics of the fluorescence decay in the mutant in the presence of DCMU (Fig. 5D and Table 1). While the loss of the hydrogen bond between D1-Glu244 and water W582 in the E224A mutant most likely contributes to the disordered acceptor side the impact is potentially amplified by the loss of a stabilizing interaction between D1-Glu244 and D2-Lys264 (Fig. 1).

Low-temperature fluorescence emission spectroscopy revealed an apparent increase in the relative amount of PS II in the E244A mutant that was not evident in the BN-PAGE data. This suggests the western blot signal with the D1 antibody was saturated whereas the sensitivity of the low temperature fluorescence emission measurements was able to determine the variation between the strains. This apparent alteration of the PS II to PS I ratio in the mutant was also evident in the room temperature fluorescence induction data in Fig. 4B, C; however, despite the apparent increase in PS II centers, on a chlorophyll basis, the E244A mutant exhibited a reduced capacity for oxygen evolution (Fig. 4A). It appears that the Ala substitution at D1-Glu244 perturbed the $Q_B$-binding site and altered the $Q_A^-/Q_A$ redox potential, particularly in the presence of bound DCMU. The increased temperature for the TL Q band and stabilized recombination kinetics for the fluorescence decay (Fig. 5D) are consistent with a positive shift in the midpoint potential for the $Q_A^-/Q_A$ couple. An increase in the midpoint potential for the $Q_A^-/Q_A$ couple is thought to reduce back reactions giving rise to $^3$Chl-mediated $^1O_2$ formation and thus may confer a degree of photoprotection [34–36]. Such a shift in the midpoint potential might arise indirectly from a conformation change but also it would be predicted if the introduced mutation destabilized the binding of bicarbonate [17]. It was expected that disrupting the pathway(s) for delivering protons to reduced $Q_B$ would result in impaired forward decay kinetics following a third actinic flash in the E244A mutant, since an increased fraction of $Q_B^{2-}(H^+)$ would be evident as a result of retarded quinol exchange at the $Q_B$ site. This, however, was not seen, with the chlorophyll decay kinetics following three actinic flashes at 4 Hz (Fig. 8) resembling the kinetics after the first flash and the observed decays were insensitive to additions of bicarbonate or formate (Figs. 7 and 8).

### 4.3. The Y246A mutant assembles PS II but exhibits an increased fraction of centers undergoing a back reaction in the absence of DCMU and is sensitive to high light

The Y246A mutant assembled PS II centers at a comparable level to that seen in isolated thylakoids from E244A cells as judged by BN-PAGE (Fig. 2C) and in E244A cells as seen in low-temperature fluorescence emission spectroscopy (Fig. 3). Variable chlorophyll fluorescence induction measurements in the presence of DCMU also indicated PS II was assembled in the Y246A mutant at a level comparable to the control but the amount of variable fluorescence was somewhat below that observed in the E244A mutant (Fig. 4C). The explanation for the difference in variable fluorescence between the E244A and Y246A cells has not yet been established. Despite the apparent wild-type or control level of PS II in Y246A cells, photoautotrophic growth was retarded in this strain, and in the E244A:Y246A double mutant (Fig. 2A), and oxygen evolution was impaired in the Y244A and E244A:Y246A strains to a greater extent than observed in the E244A mutant (Fig. 4A).

In the presence of the D1-Tyr246 to Ala substitution the chlorophyll fluorescence decay kinetics reflecting the oxidation of $Q_A^-$ were substantially more impaired than seen in the E244A strain. In the Y246A mutant the fast and intermediate phases of the decay were slowed by a factor of three relative to the control in combination with a reduction of the amplitude for both components but the amplitude for the back reaction increased six-fold to approximately 60% with the half time characteristic of the recombination reaction between $Q_A^-$ and $S_2$ (Table 1). The TL data in Fig. 6 also suggested an increased fraction of $Q_A^-$ in the Y246A cells as the apparent B band in the Y246A cells in the absence of DCMU peaked at 17.5 °C thus resembling the Q band in the presence of DCMU (Fig. 6C, F). Impaired forward electron transfer from $Q_A^-$ was also evident in the variable chlorophyll fluorescence induction where Y246A cells exhibited an initial rapid rise to an elevated J level (Fig. 4B). This suggests that the removal of the hydrogen bonds associated with Tyr 246, and both bicarbonate and water W622, introduces a perturbation of the acceptor side of PS II but does not impair PS II assembly. As was the case in the E244A mutant, the absence of any impact of formate and bicarbonate addition to the decay kinetics after a single actinic flash (Fig. 7) suggests that the structural perturbations disrupt the putative role of bicarbonate in protonation of reduced $Q_B$ via the hydrogen-bond network connecting bicarbonate to the cytosol; however, in the presence of the D1-Tyr246 to Ala substation a slight bicarbonate-reversible effect was seen in the chlorophyll fluorescence decays following the turnover of the two-electron gate after three flashes (Fig. 8).

An additional distinction between the E244A and Y246A mutants is the susceptibility of Y246A cells to high light (Figs. 9 and 10). This may suggest that the Y246A mutant produces increased levels of ROS either via $Fe^{2+}$-mediated hydroxyl radical production [37,38] or increased $^1O_2$ production via the decay of $^3[P680^+ \cdot Pheo^- \cdot]$ [9]. This putative increase in ROS in the mutant may explain the observed insertion of the premature stop codon into *psbA* in Y246A cells (Fig. S1). The inclusion of the D1-Glu244 to Ala substitution in the presence of the D1-Tyr246 to Ala substitution in the double mutant appears to offset some of the observed deleterious effects observed in the Y246A cells. There was a slight increase in the observed rate of oxygen evolution in the double mutant (Fig. 4A) while the sensitivity of oxygen-evolving activity in the E364A:Y246A cells to high light was reduced (Fig. 9B); furthermore, the impaired decay of variable fluorescence was ameliorated (Fig. 5B, Table 1). Notably the apparent stabilization of the back reaction in the presence of DCMU seen in E244A cells was retained in the E244A:Y246A double mutant (Fig. 5D).

An additional characteristic of the E244A:Y246A double mutant was the pronounced increase in variable chlorophyll fluorescence yield arising from an apparent additive effect arising from the two mutations (Figs. 4B, C and 5A, C). This observation is consistent with the altered PS II to PS I ratio apparent in the low-temperature fluorescence emission spectra (Fig. 3). This might be explained by a more oxidized plastoquinone pool in the double mutant altering the relative level of the two photosystems [39,40] or a related effect on the allocation of chlorophyll to nascent PS I or PS II complexes during biogenesis in this strain [41–45].

### 4.4. Conclusion

D1-Glu244 and D1-Tyr246 participate in a hydrogen-bond network involving several waters and the bicarbonate ligand of the non-heme iron of PS II. Replacement of these residues with Ala leads to apparent structural changes resulting in a major impact on the $Q_B$ binding site (particularly in the E244A mutant) and an increased back reaction with S2 (particularly in the Y246A mutant). The tolerance of the E244A strain towards high light is consistent with the suggestion that the presence of reduced $Q_A$ may lead to photoprotection as a result of bicarbonate dissociation [17]. The extent of the structural changes in the mutants, however, appears to disrupt the hydrogen-bond network and the ability of bicarbonate to participate in the protonation reactions associated with reduction of $Q_B$ to quinol. An increased PS II to PS I ratio is evident in the mutants, particularly in the E244A:Y246A strain, most probably as a result of a reduction in the PS I levels. Our data also suggest that the hydrogen bonds associated with waters W582 and W622 (PDB 4UB6 and Fig. 1) are important for the operation of the quinone-Fe-acceptor complex.

Supplementary data to this article can be found online at https://doi.org/10.1016/j.bbabio.2019.07.009.

## Transparency document

The Transparency document associated with this article can be found in the online version.

## Acknowledgements

We thank Jackie A. Daniels for assistance with the construction of the mutants. The research was supported by a University of Otago research grant to J.J.E.-R.; J.A.F. was supported by a University of Otago Ph.D. scholarship. I.V. acknowledges funding by the Hungarian Ministry for National Economy (GINOP-2.3.2-15-2016-0001).

## References

[1] D.J. Vinyard, G.M. Ananyev, G.C. Dismukes, Photosystem II: the reaction center of oxygenic photosynthesis, Annu. Rev. Biochem. 82 (2013) 577–606.
[2] J. Yano, V. Yachandra, $Mn_4Ca$ cluster in photosynthesis: where and how water is oxidized to dioxygen, Chem. Rev. 114 (2014) 4175–4205.
[3] T. Cardona, A. Sedoud, N. Cox, A.W. Rutherford, Charge separation in Photosystem II: a comparative and evolutionary overview, Biochim. Biophys. Acta 1817 (2012) 26–43.
[4] J. Kern, G. Renger, Photosystem II: structure and mechanism of the water:-plastoquinone oxidoreductase, Photosynth. Res. 94 (2007) 183–202.
[5] J. Kern, R. Chatterjee, I.D. Young, et al., Structure of the intermediates of Kok's photosynthetic water oxidation clock, Nature 563 (2018) 421–425.
[6] J.-R. Shen, The structure of Photosystem II and the mechanism of water oxidation, Annu. Rev. Plant Biol. 66 (2015) 23–48.
[7] Y. Umena, K. Kawakami, J.-R. Shen, N. Kamiya, Crystal structure of oxygen-evolving Photosystem II at a resolution of 1.9 Å, Nature 473 (2011) 55–60.
[8] P. Pospišil, Production of reactive oxygen species by Photosystem II as a response to light and temperature stress, Front. Plant Sci. 7 (2016) 1950, https://doi.org/10.3389/fpls.2016.01950.
[9] I. Vass, Role of charge recombination processes in photodamage and photoprotection of the Photosystem II complex, Physiol. Plant. 142 (2011) 6–16.
[10] N. Murata, S.I. Allakhverdiev, Y. Nishiyama, The mechanism of photoinhibition in vivo: re-evaluation of the roles of catalase, α-tocopherol, non-photochemical quenching, and electron transport, Biochim. Biophys. Acta 1817 (2012) 1127–1133.
[11] F. Müh, C. Glöckner, J. Hellmich, A. Zouni, Light-induced quinone reduction in Photosystem II, Biochim. Biophys. Acta 1817 (2012) 44–65.
[12] M. Suga, F. Akita, K. Hirata, G. Ueno, H. Murakami, Y. Nakajima, T. Shimizu, K. Yamashita, M. Yamamoto, H. Ago, J.-R. Shen, Native structure of Photosystem II at 1.95 Å resolution viewed by femtosecond X-ray pulses, Nature 517 (2015) 99–103.

[13] J.J. Eaton-Rye, Govindjee, Electron transfer through the quinone acceptor complex of Photosystem II after one or two actinic flashes in bicarbonate-depleted spinach thylakoid membranes, Biochim. Biophys. Acta 935 (1988) 248–257.
[14] W.L. DeLano, The PyMOL Molecular Graphics System, DeLano Scientific, Palo Alto, CA, 2001.
[15] K. Saito, A.W. Rutherford, H. Ishikita, Mechanism of proton-coupled quinone reduction in Photosystem II, Proc. Natl. Acad. Sci. U. S. A. 110 (2013) 954–959.
[16] D. Shevela, J.J. Eaton-Rye, J.-R. Shen, Govindjee, Photosystem II and the unique role of bicarbonate: a historical perspective, Biochim. Biophys. Acta 1817 (2012) 1134–1151.
[17] K. Brinkert, S. De Causmaecker, A. Krieger-Liszkay, A. Fantuzzi, A.W. Rutherford, Bicarbonate-induced redox tuning in Photosystem II for regulation and protection, Proc. Natl. Acad. Sci. U. S. A. 113 (2016) 12144–12149.
[18] J.F. Allen, J. Nield, Redox tuning in Photosystem II, Trends Plant Sci. 22 (2017) 97–99.
[19] R. Takahashi, A. Boussac, M. Sugiura, T. Noguchi, Structural coupling of a tyrosine side chain with the non-heme iron center in Photosystem II as revealed by light-induced Fourier transform infrared difference spectroscopy, Biochemistry 48 (2009) 8994–9001.
[20] J.G.K. Williams, Construction of specific mutations in Photosystem-II photosynthetic reaction center by genetic-engineering methods in *Synechocystis*-6803, Methods Enzymol. 167 (1988) 766–778.
[21] J.N. Morris, T.S. Crawford, A. Jeffs, P.A. Stockwell, J.J. Eaton-Rye, T.C. Summerfield, Whole genome re-sequencing of two 'wild-type' strains of the model cyanobacterium *Synechocystis* sp. PCC 6803, N.Z. J. Bot. 52 (2014) 36–47.
[22] J.A. Forsman, R.T. Winter, J.J. Eaton-Rye, An improved system for the targeted mutagenesis of the *psbA2* gene in *Synechocystis* sp. PCC 6803, N.Z. J. Bot. 57 (2019) 125–136.
[23] J.J. Eaton-Rye, Construction of gene interruptions and gene deletions in the cyanobacterium *Synechocystis* sp. strain PCC 6803, Methods Mol. Biol. 684 (2011) 295–312.
[24] G. MacKinney, Absorption of light by chlorophyll solutions, J. Biol. Chem. 140 (1941) 315–322.
[25] K. Cser, I. Vass, Radiative and non-radiative charge recombination pathways in Photosystem II studied by thermoluminescence and chlorophyll fluorescence in the cyanobacterium *Synechocystis* 6803, Biochim. Biophys. Acta 1767 (2007) 233–243.
[26] H. Schägger, Electrophoretic isolation of membrane-proteins from acrylamide gels, Appl. Biochem. Biotechnol. 48 (1994) 185–203.
[27] A. Stirbet, G. Yu, A.B. Rubin, Govindjee, Modeling chlorophyll *a* fluorescence transient: relation to photosynthesis, Biochemistry (Moscow) 79 (2014) 291–323.
[28] I. Vass, D. Kirilovsky, A.-L. Etienne, UV-B radiation-induced donor- and acceptor-side modifications of Photosystem II in the cyanobacterium *Synechocystis* sp. PCC 6803, Biochemistry 38 (1999) 12786–12794.
[29] H.H. Robinson, J.J. Eaton-Rye, J.J.S. van Rensen, Govindjee, The effects of bicarbonate depletion and formate incubation on the kinetics of oxidation-reduction reactions of the Photosystem II quinone acceptor complex, Z. Naturforsch. 39c (1984) 382–385.
[30] A. Sedoud, L. Kastner, N. Cox, S. El-Alaoui, D. Kirilovsky, A.W. Rutherford, Effects of formate binding on the quinone-iron electron acceptor complex of Photosystem II, Biochim. Biophys. Acta 1807 (2011) 216–226.
[31] E.-M. Aro, I. Virgin, B. Andersson, Photoinhibition of Photosystem II. Inactivation, protein damage and turnover, Biochim. Biophys. Acta 1143 (1993) 113–134.
[32] K.N. Ferreira, T.M. Iverson, K. Maghlaoui, J. Barber, S. Iwata, Architecture of the photosynthetic oxygen-evolving center, Science 303 (9) (2004) 1831–1838.
[33] V. Petrouleas, A.R. Crofts, The iron-quinone acceptor complex, in: T. Wydryzynski, K. Satoh (Eds.), Photosystem II: The Light-driven Water Plastoquinone Oxidoreductase, vol. 22, Springer, Dordrecht, 2005, pp. 177–206.
[34] F. Rappaport, M. Guergova-Kuras, P. Nixon, B.A. Diner, J. Lavergne, Kinetics and pathways of charge recombination in Photosystem II, Biochemistry 41 (2002) 8518–8527.
[35] A.W. Rutherford, A. Osyczka, F. Rappaport, Back-reactions, short-circuits, leaks and other energy wasteful reactions in biological electron transfer: redox tuning to survive life in $O_2$, FEBS Lett. 586 (2012) 603–616.
[36] I. Vass, K. Cser, Janus-faced charge recombination in Photosystem II, Trends Plant Sci. 14 (2009) 200–205.
[37] M. Miyao, M. Ikeuchi, N. Yamamoto, T. Ono, Specific degradation of the D1 protein of Photosystem II by treatment with hydrogen peroxide in darkness: implications for the mechanism of degradation of the D1 protein under illumination, Biochemistry 34 (1995) 10019–10026.
[38] P. Pospišil, A. Arató, A. Krieger-Liszkay, A.W. Rutherford, Hydroxyl radical generation by Photosystem II, Biochemistry 43 (2004) 6783–6792.
[39] T. Pfannschmidt, A. Nilsson, J.F. Allen, Photosynthetic control of chloroplast gene expression, Nature 397 (1999) 625–628.
[40] R.M. Schuurmans, J.M. Schuurmans, M. Bekker, J.C. Kromkamp, H.C.P. Matthijs, K.J. Hellingwerf, The redox potential of the plastoquinoe pool of the cyanobacterium *Synechocystis* species strain PCC 6803 is under strict homeostatic control, Plant Physiol. 165 (2014) 463–475.
[41] R. Sobotka, Making proteins green; biosynthesis of chlorophyll-binding proteins in cyanobacteria, Photosynth. Res. 119 (2014) 223–232.
[42] J. Kopečná, R. Sobotka, J. Komenda, Inhibition of chlorophyll biosynthesis at the protochlorophyllide reduction step results in the parallel depletion of Photosystem I and Photosystem II in the cyanobacterium *Synechocystis* PCC 6803, Planta 237 (2013) 497–508.
[43] V. Steccanella, M. Hansson, P.E. Jensen, Linking chlorophyll biosynthesis to a dynamic plastoquinone pool, Plant Physiol. Biochem. 97 (2015) 207–216.
[44] T.C. Crawford, J.J. Eaton-Rye, T.C. Summerfield, Mutation of Gly195 of the ChlH subunit of Mg-chelatase reduces chlorophyll and further disrupts PS II assembly in a Ycf48-deficient strain of *Synechocystis* sp. PCC 6803, Front. Plant Sci. 7 (2016) 1060, https://doi.org/10.3389/fpls.2016.01060.
[45] S. Hollingshead, J. Kopečná, D.R. Armstrong, et al., Synthesis of chlorophyll-binding proteins in a fully segregated Δ*ycf54* strain of the cyanobacterium *Synechocystis* sp. PCC 6803, Front. Plant Sci. 7 (2016) 292, https://doi.org/10.3389/fpls.2016.00292.